metals

MDPI

Article

In Situ Generated Shear Bands in Metallic Glass Investigated by Atomic Force and Analytical Transmission Electron Microscopy

Harald Rösner [1,*], Christian Kübel [2,3,4], Stefan Ostendorp [1] and Gerhard Wilde [1]

[1] Institut für Materialphysik, Westfälische Wilhelms-Universität Münster, Wilhelm-Klemm-Str. 10, 48149 Münster, Germany; stefan.ostendorp@uni-muenster.de (S.O.); gwilde@uni-muenster.de (G.W.)
[2] Institute of Nanotechnology (INT), Karlsruhe Institute of Technology (KIT), Hermann-von-Helmholtz-Platz 1, 76344 Eggenstein-Leopoldshafen, Germany; christian.kuebel@kit.edu
[3] Karlsruhe Nano Micro Facility, Karlsruhe Institute of Technology, 76344 Eggenstein-Leopoldshafen, Germany
[4] Material-und Geowissenschaften, Technische Universität Darmstadt, Alarich-Weiss-Str. 2, 64287 Darmstadt, Germany
* Correspondence: rosner@uni-muenster.de

Abstract: Plastic deformation of metallic glasses performed at temperatures well below the glass transition proceeds via the formation of shear bands. In this contribution, we investigated shear bands originating from in situ tensile tests of $Al_{88}Y_7Fe_5$ melt-spun ribbons performed under a transmission electron microscope. The observed contrasts of the shear bands were found to be related to a thickness reduction rather than to density changes. This result should alert the community of the possibility of thickness changes occurring during in situ shear band formation that may affect interpretation of shear band properties such as the local density. The observation of a spearhead-like shear front suggests a propagation front mechanism for shear band initiation here.

Keywords: metallic glass; shear band; in situ TEM

Citation: Rösner, H.; Kübel, C.; Ostendorp, S.; Wilde, G. In Situ Generated Shear Bands in Metallic Glass Investigated by Atomic Force and Analytical Transmission Electron Microscopy. *Metals* **2022**, *12*, 111. https://doi.org/10.3390/met12010111

Academic Editor: Alberto Moreira Jorge Junior

Received: 23 November 2021
Accepted: 3 January 2022
Published: 6 January 2022

1. Introduction

Deformation processes in metallic glasses are different from those in crystalline materials due to the absence of a periodic lattice. Deformation tests on metallic glasses well below the glass transition temperature using deformation rates less than 10^{-2} have shown that the plastic flow is confined to narrow regions called shear bands when the applied strain exceeds the elastic range [1–6]. Shear bands are a type of material instability and thus a precursor to material failure. Whereas shear bands typically have widths of 5–20 nm [7–12], larger widths in the range of 100–200 nm have also been reported [13–16].

It is commonly thought that the shear band core is associated with a structural change due to shear dilatation, implying a volume increase and thus a change in density [3–5,7–9,14–28]. Therefore, shear band cores are softer [26,29] than the surrounding matrix, allowing the applied shear strains to be accommodated via slip. An important issue is thus the quantification of free volume [24] or density inside shear bands [11]. Whereas the interpretation of contrast changes in transmission electron microscopy (TEM) is often complicated [30–32], investigations on $Al_{88}Y_7Fe_5$ metallic glass deformed ex situ by cold rolling have revealed local contrast changes within shear bands, which have been successfully determined as density changes using high-angle annular dark field scanning transmission electron microscopy (HAADF-STEM) in combination with foil thickness measurements [11,33,34]. In this study, we investigated in situ generated shear bands formed under tension in the TEM and show, by accompanying thickness and surface measurements, that their contrasts are related to thickness reduction, unlike the ex situ samples where no change in thickness was observed. The

results for the in situ sample are discussed with respect to the thin foil geometry during in situ straining under TEM.

2. Materials and Methods

Fully amorphous ribbons of $Al_{88}Y_7Fe_5$ (composition in atomic percent) with an average thickness of 40 µm were produced by melt spinning. For more details, see Ref. [35]. TEM specimens were prepared by twinjet electropolishing (Tenupol-5, Struers, Copenhagen, Denmark) using HNO_3:CH_3OH in a ratio of 1:2 at −22 °C, applying voltages of about −10.5 V. The in situ TEM study was performed using an FEI Titan 80–300 image-corrected transmission electron microscope equipped with a post-column energy filter (Tridiem 863 Gatan Imaging Filter) operated at 300 kV in STEM mode. HAADF images and electron-energy loss (EEL) spectra were collected with an HAADF detector (Fischione model 3000) and a slow-scan CCD camera (Gatan US 1000) using the following parameters: camera length of 102 mm, convergence semi-angle α of 9.5 mrad, collection semi-angle β of 3 mrad, an entrance aperture of 2 mm, an energy dispersion of 0.2 eV/channel, an acquisition time of 400 ms, and a nominal spot size of 0.5 nm. Shear bands were produced by in situ straining of the ribbons at ambient temperature using a single-tilt tensile stage (Gatan Model 672) [36]. An atomic force microscope (AFM, Park XE 100) operated in non-contact (NC) AFM mode was used to measure the topography of the sheared zones after deformation. The HAADF-STEM signal (electrons collected by the HAADF detector between 60 and 200 mrad) can be used to gain information about the density/volume change [11,33]. The cross-section for HAADF scattering approaches the (un)screened Rutherford cross-section, which is in the range of $Z^{1.7–2}$ [37].

An exponential decrease in transmission of the STEM signal with increasing mass thickness $x = \rho \cdot t$ has been found for amorphous specimens [38,39]. The dark-field intensity I/I_0 can be formulated as:

$$\frac{I}{I_0} = \left[1 - exp\left(-\frac{\rho \cdot t}{x_k}\right)\right] \quad (1)$$

where ρ is the density, t is the foil thickness, and x_k is the contrast thickness. For a constant contrast thickness x_k and a small argument [11], the HAADF-STEM signal I/I_0 scales with the mass thickness ($x = \rho \cdot t$):

$$\frac{I}{I_0} \propto \frac{\rho \cdot t}{x_k} \quad (2)$$

Thus to determine the density, the corresponding local foil thickness t has also to be measured [40]. This can be achieved by EEL spectroscopy (EELS) using the information from the low-loss region. The refractive index-corrected Kramers–Kronig sum rule, according to Iakoubovskii et al. [41], was used to calculate the corresponding foil thickness profiles, as it is thought to provide more accurate values for the foil thickness in amorphous materials than the log-ratio method [40]. It analyses the single scattering distribution S(E), which is obtained from the EEL spectrum. Plural scattering was removed before the thickness computation from the EEL spectra using the Fourier-log method [42]. However, there is a systematical error for the absolute foil thickness of ±20% [40,43]. Finally, a density change could be derived after Equation (2) by measuring the contrast signal (intensity) together with the corresponding foil thickness. To avoid contamination during measurements, the samples were plasma-cleaned in pure Ar prior to analysis.

3. Results

During the in situ elongation of the sample, the edge of the electron transparent area was observed at low magnification in STEM mode. Scanning at low magnification reduces irradiation effects [44] such as nanocrystallization [45] and provides a larger field of view. When shear bands occurred, the deformation was immediately stopped. Figure 1a displays an HAADF-STEM image showing shear bands triggered by the elongation of the foil. Most of them were torn open. Note that no apparent shear steps emerging from the shear bands at the edge of the thin foil were observed. The framed area shows a shear band with

a branch. The first part of the shear band appears bright as a result of the shear band having cracked open and closed again. Figure 1b shows an enlarged view of the tip of the horizontally propagating part of the shear band, which is darker than the surrounding matrix. The shear front exhibits a spearhead-like shape, as proposed in Ref. [46]. The visible width of the shear band varies around 75 nm due to an interplay between materials' flaws and the complex local stress fields [47] operating in the thin regions of the TEM sample, until it tapers toward the tip (marked with a cross). White lines indicate the position of the line scans performed in nanometer steps across the shear band.

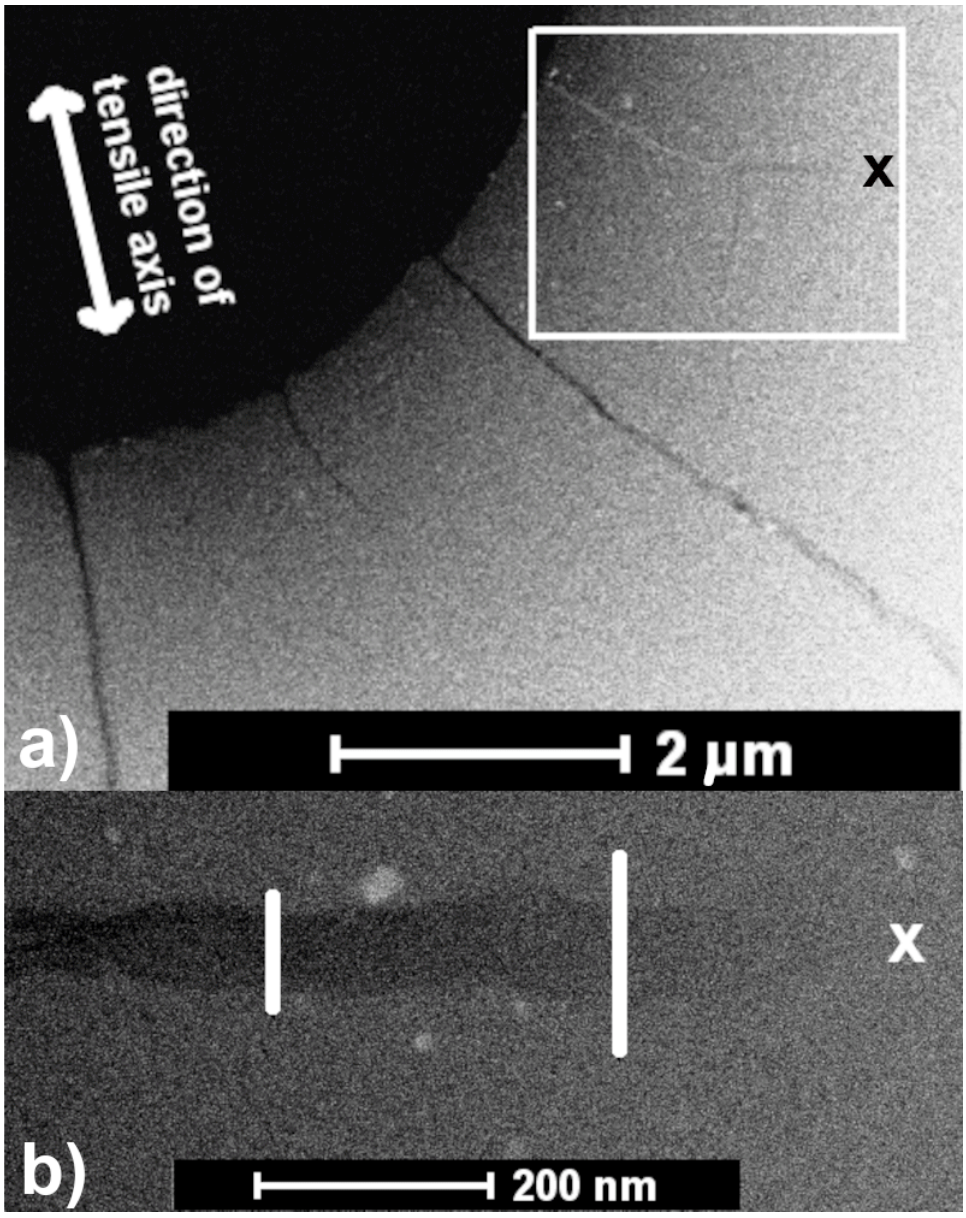

Figure 1. (**a**) HAADF-STEM image showing an overview of shear bands generated during an in situ TEM tensile test of an $Al_{88}Y_7Fe_5$ melt-spun ribbon. The framed area shows a shear band with a branch. (**b**) Enlarged view of the tip of the horizontally propagating part of the shear band. White lines indicate the position of the line profiles performed from bottom to top across the shear band. The position marked X indicates the shear band tip, revealing a spearhead-like shape.

The HAADF-STEM signals corrected for the vacuum off-set are shown in Figure 2a,c. The signals decreased from the matrix level by 15.7% ± 1.9% and 4.8% ± 1.9%. The corresponding thickness profiles across the shear band are plotted in Figure 2b,d, showing

drops of 16% ± 2.8% and 5.5% ± 2%. Typical EEL spectra used for the thickness calculations are shown in Figure 3, displaying zero loss and plasmon peaks. The higher zero loss peak relative to the plasmon peaks shows that the shear band is thinner than the matrix. All shear band profiles shown in Figure 2 indicate a meniscus-like relief with a change in thickness across the shear band.

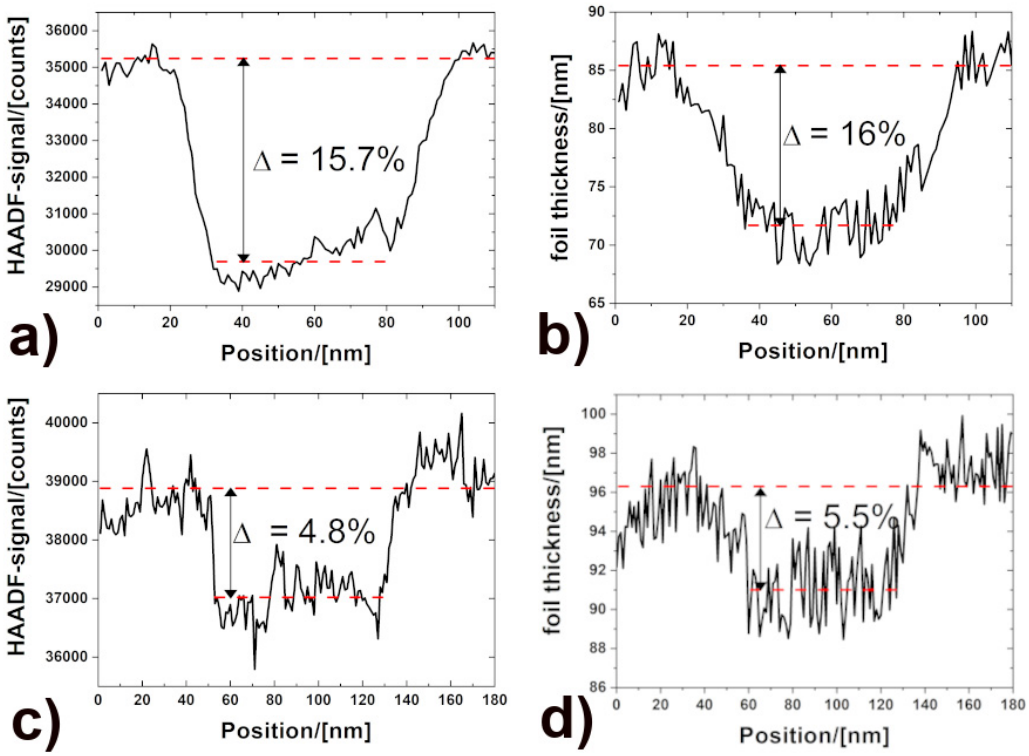

Figure 2. Corresponding line profiles as indicated in Figure 1b. (**a**) HAADF-STEM profile across the shear band corresponding to the shorter line, showing a reduction of 15.7% ± 1.9%. (**b**) Corresponding thickness profile showing a reduction of 16% ± 2.8%. (**c**) HAADF-STEM profile across the shear band corresponding to the longer line showing a drop of 4.8% ± 1.9%. (**d**) Corresponding thickness profile showing a reduction of 5.5% ± 2%.

The thickness change also varies along the shear band, with the relative thickness change being less near the shear band tip. Since both intensity and thickness profiles in Figure 2 show similar drops within the experimental error, the contrast change can be attributed, according to Equation (2), to thickness reductions rather than to density changes [7,14,48].

In order to prove these findings by an independent technique, the surface of the in situ sample was investigated by non-contact AFM after deformation. The obtained profiles shown in Figure 4 revealed a similar topology in nearby but different shear bands from that observed by analytical TEM, confirming the decrease in the sample thickness at the shear bands.

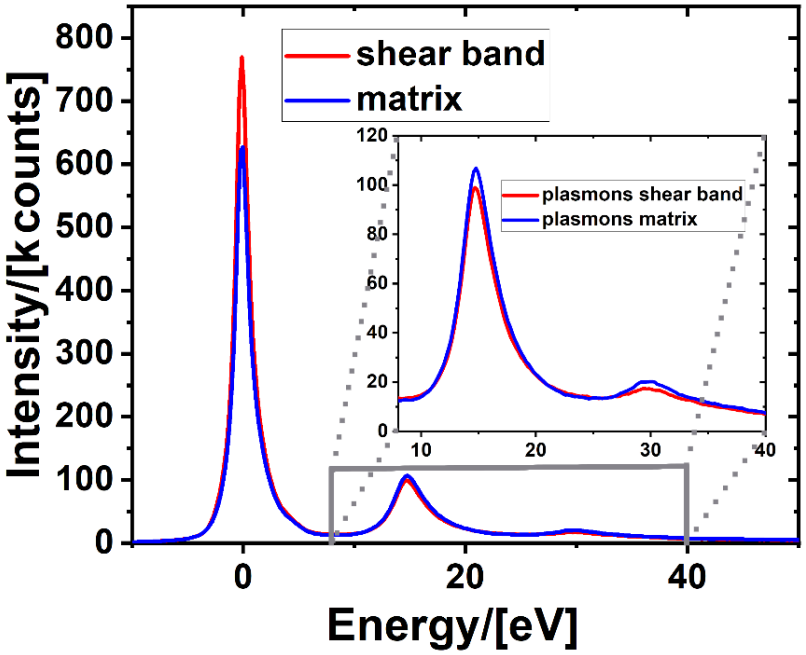

Figure 3. Representative EEL spectra taken from the matrix (blue) and the shear band (red) corresponding to the shorter line scan in Figure 1b, showing zero loss and plasmon peaks. The low-loss part (0–50 eV) was used for the thickness calculations. The inset shows an enlarged view of the plasmons. Note the difference in peak heights between the matrix and shear band.

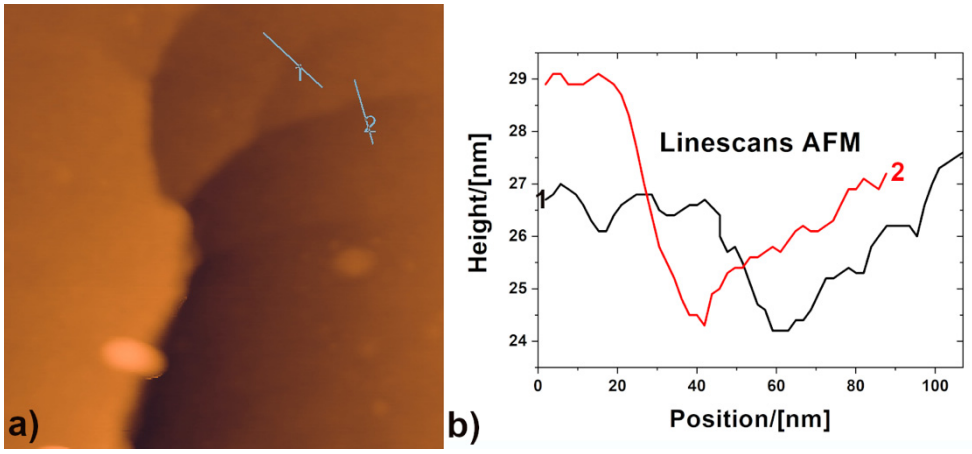

Figure 4. (**a**) NC-AFM performed on the in situ sample after deformation. Two line scans (blue lines) were measured across the in situ generated shear band branches. (**b**) Corresponding profiles of the line scans indicated in (**a**), revealing a thickness reduction in the form of a meniscus across the shear bands.

4. Discussion

The following discussion focuses on three issues: the spearhead-like shear front, the thickness reduction, and the lack of alternating density changes in the in situ shear bands. One unsolved and still heavily debated issue with respect to the inhomogeneous deformation of metallic glasses is the shear band initiation [4–6]. Is this a percolative process simultaneously happening across the entire shear plane [49], or a mechanism controlled by a propagating shear front [46,50–53]? The observation of a spearhead-like shear front suggests that the shear band initiation in this case was mediated by a propagating shear front, which includes the activation and percolation of individual shear transformation zones [50,51,54].

The thickness reduction was observed in the form of a meniscus or groove with the thickness varying along and across the shear band. This shape is most probably a consequence of necking of the shear-softened zone under the reduced constraint of a 2D geometry in the thin foil, thus displaying a snapshot before failure that would occur upon continued deformation.

Note that previous results on ex situ samples showed negligible thickness changes; therefore, on the basis of Equation (2), the HAADF contrast changes were interpreted as density changes [11,33,34]. Here, in the in situ sample, we observed thickness changes in the shear band of the same order as the HAADF contrast changes and, therefore, on the basis of Equation (2), we concluded that the change in HAADF contrast arises either completely or almost completely from the thickness changes. These differences illustrate the importance of checking for thickness changes when interpreting contrast changes as density changes.

Whereas distinct alternating density changes were observed in the shear bands of ex situ samples produced by cold rolling [11,33,34,55] or simulation [56], the current in situ investigation did not show such alternating contrast reversals. It was mentioned above (see the Results) that bright contrast was observed in one of the shear bands, as shown in Figure 1. However, this contrast is to be distinguished from the alternating contrast changes, since the bright contrast in the in situ experiment occurred due to a shear band having cracked open and closed again. Two possible explanations for the lack of alternating contrast changes are, first, the density changes are present but not discernible due to the thickness reduction and/or tapering of the shear bands; second, in situ generated shear bands rip before such features can develop, which implies that there are two stages involved. In the first stage, the shear front forms a rejuvenated and thus softened path including the activation and percolation of individual shear transformation zones. This paves the way for the second stage, where shearing along the already softened path occurs [4,52]. In support of this scenario, we refer to the lack of shear steps emerging from the shear bands at the edge of the thin foil, which suggests that the in situ generated shear bands display the first stage of shear band formation.

5. Conclusions

In summary, we showed that in situ generated shear bands have a meniscus-like thickness reduction, which is most probably a consequence of necking of the shear-softened zone under the reduced constraint of a 2D geometry in the thin foil. This result should alert the community to the possibility of thickness changes occurring during in situ shear band formation, which may affect the interpretation of shear band properties such as the local density. The observation of a spearhead-like shear front suggests a propagation front mechanism for the shear band initiation here.

Author Contributions: Conceptualization, H.R.; Data curation, H.R.; Funding acquisition, G.W.; Investigation, H.R., C.K. and S.O.; Visualization, H.R.; Writing–original draft, H.R.; Writing–review & editing, C.K., S.O. and G.W. All authors contributed equally to this work. All authors have read and agreed to the published version of the manuscript.

Funding: We gratefully acknowledge financial support by the DFG via WI 1899/29-1 (Coupling of irreversible plastic rearrangements and heterogeneity of the local structure during deformation of metallic glasses, project number 325408982). The DFG is further acknowledged for funding our TEM equipment via the Major Research Instrumentation Program under INST 211/719-1 FUGG, project number 288115331.

Institutional Review Board Statement: Not applicable.

Informed Consent Statement: Not applicable.

Data Availability Statement: The original data of this study are available from the corresponding author upon reasonable request.

Acknowledgments: This work was partially carried out with support of the Karlsruhe Nano Micro Facility (KNMFi, www.knmf.kit.edu (accessed on 23 November 2021)), a Helmholtz research infrastructure at Karlsruhe Institute of Technology (KIT, www.kit.edu (accessed on 23 November 2021)).

Conflicts of Interest: The authors declare that they have no known competing financial interest or personal relationship that could influence the work reported in this paper.

References

1. Pampillo, C. Localized shear deformation in a glassy metal. *Scr. Metall.* **1972**, *6*, 915–917. [CrossRef]
2. Spaepen, F. A microscopic mechanism for steady state inhomogeneous flow in metallic glasses. *Acta Metall.* **1977**, *25*, 407–415. [CrossRef]
3. Schuh, C.A.; Hufnagel, T.C.; Ramamurty, U. Mechanical behavior of amorphous alloys. *Acta Mater.* **2007**, *55*, 4067–4109. [CrossRef]
4. Greer, A.L.; Cheng, Y.Q.; Ma, E. Shear bands in metallic glasses. *Mater. Sci. Eng. R Rep.* **2013**, *74*, 71–132. [CrossRef]
5. Maaß, R.; Löffler, J.F. Shear-Band Dynamics in Metallic Glasses. *Adv. Funct. Mater.* **2015**, *25*, 2353–2368. [CrossRef]
6. Hufnagel, T.C.; Schuh, C.A.; Falk, M. Deformation of metallic glasses: Recent developments in theory, simulations, and experiments. *Acta Mater.* **2016**, *109*, 375–393. [CrossRef]
7. Donovan, P.E.; Stobbs, W.M. The structure of shear bands in metallic glasses. *Acta Metall.* **1981**, *29*, 1419–1436. [CrossRef]
8. Li, J.; Spaepen, F.; Hufnagel, T.C. Nanometre-scale defects in shear bands in a metallic glass. *Philos. Mag. A* **2002**, *82*, 2623–2630. [CrossRef]
9. Zhang, Y.; Greer, A.L. Thickness of shear bands in metallic glasses. *Appl. Phys. Lett.* **2006**, *89*, 071907. [CrossRef]
10. Shao, Y.; Yang, G.N.; Yao, K.F.; Liu, X. Direct experimental evidence of nano-voids formation and coalescence within shear bands. *Appl. Phys. Lett.* **2014**, *105*, 181909. [CrossRef]
11. Rösner, H.; Peterlechner, M.; Kübel, C.; Schmidt, V.; Wilde, G. Density changes in shear bands of a metallic glass determined by correlative analytical transmission electron microscopy. *Ultramicroscopy* **2014**, *142*, 1–9. [CrossRef]
12. Hieronymus-Schmidt, V.; Rösner, H.; Wilde, G.; Zaccone, A. Shear banding in metallic glasses described by alignments of Eshelby quadrupoles. *Phys. Rev. B* **2017**, *95*, 134111. [CrossRef]
13. Pauly, S.; Lee, M.H.; Kim, D.H.; Kim, K.B.; Sordelet, D.J.; Eckert, J. Crack evolution in bulk metallic glasses. *J. Appl. Phys.* **2009**, *106*, 103518. [CrossRef]
14. Liu, C.; Roddatis, V.; Kenesei, P.; Maaß, R. Shear-band thickness and shear-band cavities in a Zr-based metallic glass. *Acta Mater.* **2017**, *140*, 206–216. [CrossRef]
15. Maaß, R. Beyond serrated flow in bulk metallic glasses: What comes next? *Metall. Mater. Trans. A* **2020**, *51*, 5597–5605. [CrossRef]
16. Liu, C.; Ikeda, Y.; Maaß, R. Strain-dependent shear-band structure in a Zr-based bulk metallic glass. *Scr. Mater.* **2021**, *190*, 75–79. [CrossRef]
17. Li, J.; Wang, Z.L.; Hufnagel, T.C. Characterization of nanometer-scale defects in metallic glasses by quantitative high-resolution transmission electron microscopy. *Phys. Rev. B* **2002**, *65*, 144201. [CrossRef]
18. Jiang, W.H.; Atzmon, M. The effect of compression and tension on shear-band structure and nanocrystallization in amorphous Al90Fe5Gd5: A high-resolution transmission electron microscopy study. *Acta Mater.* **2003**, *51*, 4095–4105. [CrossRef]
19. Jiang, W.H.; Pinkerton, F.E.; Atzmon, M. Mechanical behavior of shear bands and the effect of their relaxation in a rolled amorphous Al-based alloy. *Acta Mater.* **2005**, *53*, 3469–3477. [CrossRef]
20. Hajlaoui, K.; Yavari, A.R.; Doisneau, B.; LeMoulec, A.; Vaughan, G.; Greer, A.L.; Inoue, A.; Zhang, W.; Kvick, Å. Shear delocalization and crack blunting of a metallic glass containing nanoparticles: In situ deformation in TEM analysis. *Scr. Mater.* **2006**, *54*, 1829–1834. [CrossRef]
21. Ishii, A.; Hori, F.; Iwase, A.; Fukumoto, Y.; Yokoyama, Y.; Konno, T.J. Relaxation of free volume in Zr50Cu40Al10 bulk metallic glasses studied by positron annihilation measurements. *Mater. Trans.* **2008**, *49*, 1975–1978. [CrossRef]
22. Guan, P.; Chen, M.; Egami, T. Stress-temperature scaling for steady-state flow in metallic glasses. *Phys. Rev. Lett.* **2010**, *104*, 205701. [CrossRef]
23. Lechner, W.; Puff, W.; Wilde, G.; Würschum, R. Vacancy-type defects in amorphous and nanocrystalline Al alloys: Variation with preparation route and processing. *Scr. Mater.* **2010**, *62*, 439–442. [CrossRef]
24. Klaumünzer, D.; Lazarev, A.; Maaß, R.; Dalla Torre, F.H.; Vinogradov, A.; Löffler, J.F. Probing shear-band initiation in metallic glasses. *Phys. Rev. Lett.* **2011**, *107*, 185502. [CrossRef]
25. Miller, M.K.; Longstreth-Spoor, L.; Kelton, K.F. Detecting density variations and nanovoids. *Ultramicroscopy* **2011**, *111*, 469–472. [CrossRef]
26. Pan, J.; Chen, Q.; Liu, L.; Li, Y. Softening and dilatation in a single shear band. *Acta Mater.* **2011**, *59*, 5146–5158. [CrossRef]
27. Shao, H.; Xu, Y.; Shi, B.; Yu, C.; Hahn, H.; Gleiter, H.; Li, J. High density of shear bands and enhanced free volume induced in Zr70Cu20Ni10 metallic glass by high-energy ball milling. *J. Alloys Compd.* **2013**, *548*, 77–81. [CrossRef]
28. Liu, C.; Cai, Z.; Xia, X.; Roddatis, V.; Yuan, R.; Zuo, J.M.; Maaß, R. Shear-band structure and chemistry in a Zr-based metallic glass probed with nano-beam x-ray fluorescence and transmission electron microscopy. *Scr. Mater.* **2019**, *169*, 23–27. [CrossRef]
29. Bei, H.; Xie, S.; George, E.P. Softening caused by profuse shear banding in a bulk metallic glass. *Phys. Rev. Lett.* **2006**, *96*, 105503. [CrossRef]

30. Hirsch, P.B.; Howie, A.; Nicholson, R.B.; Pashley, D.W.; Whelan, M.J. *Electron Microscopy of Thin Crystals*, 1st ed.; Butterworths: London, UK, 1965.
31. Edington, J.W. *Practical Electron Microscopy in Materials Science: Interpretation of Transmission Electron Micrographs*, 1st ed.; The Macmillan Press Ltd.: London/Basingstoke, UK, 1975.
32. Williams, D.B.; Carter, C.B. *The Transmission Electron Microscope*, 1st ed.; Springer: Boston, MA, USA, 1996.
33. Schmidt, V.; Rösner, H.; Peterlechner, M.; Wilde, G.; Voyles, P.M. Quantitative measurement of density in a shear band of metallic glass monitored along its propagation direction. *Phys. Rev. Lett.* **2015**, *115*, 035501. [CrossRef]
34. Grove, M.; Peterlechner, M.; Rösner, H.; Imlau, R.; Zaccone, A.; Wilde, G. Plasmon energy losses in shear bands of metallic glass. *Ultramicroscopy* **2021**, *223*, 113220. [CrossRef]
35. Bokeloh, J.; Boucharat, N.; Rösner, H.; Wilde, G. Primary crystallization in Al-rich metallic glasses at unusually low temperatures. *Acta Mater.* **2010**, *58*, 3919–3926. [CrossRef]
36. Rösner, H.; Boucharat, N.; Markmann, J.; Padmanabhan, K.A.; Wilde, G. In situ transmission electron microscopic observations of deformation and fracture processes in nanocrystalline palladium and Pd90Au10. *Mater. Sci. Eng. A* **2009**, *525*, 102–106. [CrossRef]
37. Pennycook, S.J. Structure determination through Z-contrast microscopy. In *Advances in Imaging and Electron Physics*; Elsevier: Amsterdam, The Netherlands, 2002; Volume 123, pp. 173–206.
38. Reimer, L.; Hagemann, P. Recording of mass thickness in scanning transmission electron microscopy. *Ultramicroscopy* **1976**, *2*, 297–301. [CrossRef]
39. Reimer, L.; Kohl, H. *Transmission Electron Microscopy: Physics of Image Formation*, 5th ed.; Springer: New York, NY, USA, 2008; p. 202.
40. Malis, T.; Cheng, S.C.; Egerton, R.F. EELS log-ratio technique for specimen-thickness measurement in the TEM. *J. Electron Microsc. Tech.* **1988**, *8*, 193–200. [CrossRef]
41. Iakoubovskii, K.; Mitsuishi, K.; Nakayama, Y.; Furuya, K. Thickness measurements with electron energy loss spectroscopy. *Microsc. Res. Tech.* **2008**, *71*, 626–631. [CrossRef]
42. Egerton, R.F.; Williams, B.G.; Sparrow, T.G. Fourier deconvolution of electron energy-loss spectra. *Proc. R. Soc. Lond. A Math. Phys. Sci.* **1985**, *398*, 395–404.
43. Egerton, R.F. *Electron Energy-Loss Spectroscopy in the Electron Microscope*, 3rd ed.; Springer: New York, NY, USA, 2011.
44. Mačković, M.; Niekiel, F.; Wondraczek, L.; Bitzek, E.; Spiecker, E. In situ mechanical quenching of nanoscale silica spheres in the transmission electron microscope. *Scr. Mater.* **2016**, *121*, 70–74. [CrossRef]
45. Wilde, G.; Rösner, H. Nanocrystallization in a shear band: An in situ investigation. *App. Phys. Lett.* **2011**, *98*, 251904. [CrossRef]
46. Shimizu, F.; Ogata, S.; Li, J. Yield point of metallic glass. *Acta Mater.* **2006**, *54*, 4293–4298. [CrossRef]
47. Chen, S.H.; Li, T.; Chang, W.J.; Yang, H.D.; Zhang, J.C.; Tang, H.H.; Feng, S.D.; Wu, F.F.; Wu, Y.C. On the formation of shear bands in a metallic glass under tailored complex stress fields. *J. Mater. Sci. Technol.* **2020**, *53*, 112–117. [CrossRef]
48. De Hosson, J.T.M. Advances in transmission electron microscopy: In situ straining and in situ compression experiments on metallic glasses. *Microsc. Res. Tech.* **2009**, *72*, 250–260. [CrossRef]
49. Packard, C.E.; Schuh, C.A. Initiation of shear bands near a stress concentration in metallic glass. *Acta Mater.* **2007**, *55*, 5348–5358. [CrossRef]
50. Şopu, D.; Stukowski, A.; Stoica, M.; Scudino, S. Atomic-level processes of shear band nucleation in metallic glasses. *Phys. Rev. Lett.* **2017**, *119*, 195503. [CrossRef] [PubMed]
51. Şopu, D.; Scudino, S.; Bian, X.L.; Gammer, C.; Eckert, J. Atomic-scale origin of shear band multiplication in heterogeneous metallic glasses. *Scr. Mater.* **2020**, *178*, 57–61. [CrossRef]
52. Cao, A.J.; Cheng, Y.Q.; Ma, E. Structural processes that initiate shear localization in metallic glass. *Acta Mater.* **2009**, *57*, 5146–5155. [CrossRef]
53. Yang, Y.; Liu, C.T. Size effect on stability of shear-band propagation in bulk metallic glasses: An overview. *J. Mater. Sci.* **2012**, *47*, 55–67. [CrossRef]
54. Argon, A.S. Plastic deformation in metallic glasses. *Acta Metall.* **1979**, *27*, 47–58. [CrossRef]
55. Balachandran, S.; Orava, J.; Köhler, M.; Breen, A.J.; Kaban, I.; Raabe, D.; Herbig, M. Elemental re-distribution inside shear bands revealed by correlative atom-probe tomography and electron microscopy in a deformed metallic glass. *Scr. Mater.* **2019**, *168*, 14–18. [CrossRef]
56. Hassani, M.; Lagogianni, A.E.; Varnik, F. Probing the degree of heterogeneity within a shear band of a model glass. *Phys. Rev. Lett.* **2019**, *123*, 195502. [CrossRef] [PubMed]